Proceedings World Geothermal Congress 2026
Calgary, Canada, June 8 – 11, 2026

Comprehensive Assessment of the DEL-GT-02 Drilling Operations at TU Delft Campus

Alexis Koulidis[1*], Susanne Laumann[1] and Philip J. Vardon[1]
Delft University of Technology, Faculty of Civil Engineering and Geosciences, Delft, Netherlands[1*]
k.a.koulidis@tudelft.nl

Keywords: well design, drilling operations, drilling automation

ABSTRACT

The geothermal energy sector relies on drilling deep wells, with borehole instability and consequential remedial actions impacting project profitability substantially. This study focuses on a particularly challenging section encountered during the drilling of the injector well (DEL-GT-02) of the Geothermie Delft doublet on the TU Delft campus, specifically addressing challenges related to wellbore instability and collapse. The paper presents a framework to automate the analysis of the actual drilling operations and provide an assessment of the wellbore condition. Essential drilling data required to perform the analysis are well trajectory, drilling fluid properties, drilling parameters (WOB, RPM, etc.), and the bottomhole assembly (BHA) design. A data quality framework is utilized to automate the recognition of the operation and separate the data into time and depth domains. Appropriate physics-based modelling including wellbore reconstruction, drilling hydraulics and torque and drag, allows comparison with the measured variables. Recorded torque spikes and losses are utilized to evaluate the performance of the algorithm. This study demonstrates an automated framework for analysing drilling data, integrated with physics-based modelling to assess wellbore quality. The approach enables comparison between modeled and actual drilling parameters to identify intervals and trends where discrepancies occur, providing insights relevant to the drilling operations.

1 INTRODUCTION

In 2023, a geothermal doublet was drilled on the TU Delft campus in the Netherlands by the Geothermie Delft consortium and is scheduled to provide heat by the end of 2025 (Vardon et al., 2024; Voskov et al., 2024). The injector well (DEL-GT-02) encountered several challenges while drilling the deeper part of the 12.25-in section, which resulted in wellbore collapse. The well required two sidetracks to reach the target depth and have a functional well (Vardon et al., 2024).

Geothermal well engineering shares many technical challenges with oil and gas drilling operations. The quality of a wellbore, corresponding to tight spots and hole geometry, is influenced by various factors during drilling, including drilling fluid properties, drilling parameters, mechanical vibrations, geomechanical conditions, and wellbore trajectory (Van Oort, 2003; Zoback, 2010). Furthermore, drilling practices such as wiper trips and well circulation help maintain wellbore quality, whereas backreaming may have a negative impact (Yarim et al., 2010).

Several methods have been developed to evaluate casing run feasibility, for example, Marbun et al. (2014) introduced a casing while drilling (CWD) study and the required considerations to reduce drilling time and risk; Samuel et al. (2024) focused on utilising real-time drilling conditions and survey data to provide runnability metrics; and Montes et al. (2025) proposed a digital tool to automate the analysis process that assesses the potential for casing run failure.

The overall wellbore condition can be assessed by several indicators, including torque, drag, overpulls, cuttings loading and drilling hydraulics (Johancsik et al., 1984; Van Oort, 2003). Over the past decade, real-time operations have supported decision-making during well drilling by incorporating physics-based modelling and machine learning (ML) models, which were trained on large datasets (Cayeux and Daireaux, 2009; Ng et al., 2019; Richard et al., 2022; Chi et al., 2023). Adoption is, however, limited due to the need for robust communication networks and platforms, which are often not available at many drilling locations.

Dynamic drilling simulation can serve as an intelligent system for identifying and analysing differences between model predictions and actual measurements during drilling operations. Conventional simulations of wells consist of static modelling for a set of variables that represent average values for a sector. This way of modelling considers the BHA design, drilling fluid properties, etc., but does not consider the actual drilling variables that were used to drill the well, i.e. the actual flow rates, mud motor torque and differential pressure. This paper focuses on applying an automated framework that integrates drilling data analytics with dynamic

drilling simulations, including drilling hydraulics and torque-and-drag analysis, to provide insights into the challenges encountered during the operation.

This work focuses on the 12.25-in section of the Geothermie Delft DEL-GT-02 injector well, where a wellbore collapse was encountered during pull-out-of-hole (POOH). The objective of this research is to evaluate whether the event could have been predicted by comparing dynamic drilling simulations with actual field measurements. The objective was to assess the overall drilling process to observe any indications or early signs of wellbore collapse. An automated framework was applied that integrates drilling data analytics with dynamic drilling simulations, including hydraulics and torque & drag analyses, to compare modelled and measured parameters and provide insights into the challenges encountered during the operation.

2 CASE STUDY - GEOTHERMIE DELFT DEL-GT-02

The data utilized for the current case study are obtained from the injector well DEL-GT-02 of the Geothermie Delft geothermal project located on the TU Delft campus in the Netherlands, which is a doublet system targeting a sedimentary reservoir at approximately 2.1 km depth. It is a deviated well with a complex lithology with different bottomhole assemblies (BHA) utilized for each section. As shown in Figure 1, after drilling the surface section, a 13-3/8-in casing was run to 841 m. Following this, a 12 1/4" section was drilled between 841 m and the target depth (TD) of 2637 m (measured depth). Once TD was reached, while performing POOH, the drill string became stuck and was unable to POOH, with the BHA at approximately 1431 m. The decision was made to sever the BHA and plugback for a sidetrack.

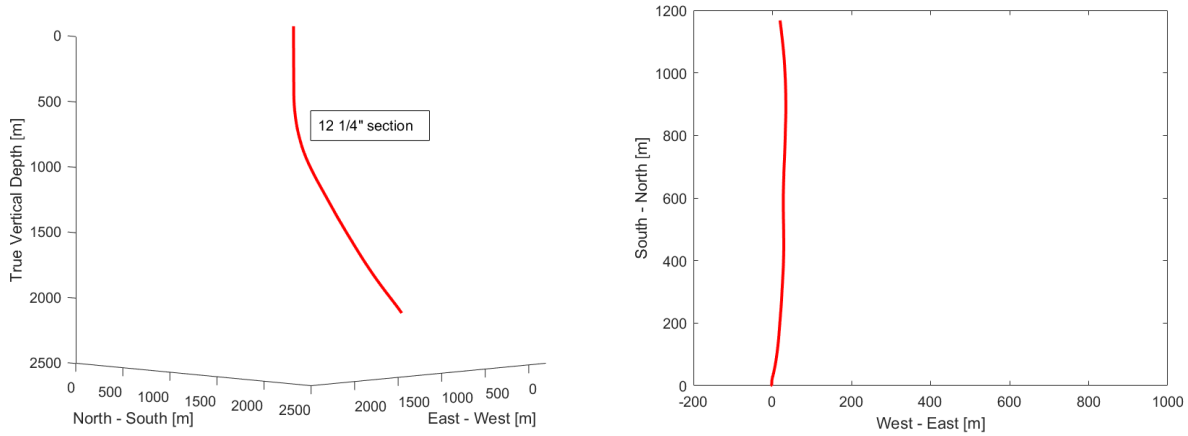


Figure 1. Well design and actual survey for DEL-GT-02

3 DATA WORKFLOW

The workflow from data extraction to dynamic modelling is presented in Figure 2. Data visualisation and extraction are performed using various libraries in Python. The datasets are exported for each day, with the required attributes, and subsequently compiled into a single file to perform an integrated analysis of the entire section. Selected steps of this workflow were adapted from Koulidis et al. (2023) and Koulidis and Ahmed (2024) to perform data quality checks, operations recognition and obtain the differential pressure from the mud motor.

A key aspect of the current methodology is to utilize unprocessed drilling data to evaluate the overall drilling process. Drilling is not a continuous process, with various operations taking place while drilling a well. Drilling data is stored in various formats and often several variables are calculated, and others are measured. In addition, drilling data might be distributed to different parties prior to storage. Thus, data quality is crucial to ensuring that measurements and calculated values are accurate and reliable.

Initially, calculated values (that were reported by the drilling monitoring system) are recalculated at a higher frequency. The data is then checked for quality. The resulting dataset is then labelled in both accurate time and depth domains, enabling a comprehensive assessment of the drilling process. In this study, the drilling process is assessed using dynamic modeling, incorporating both drilling hydraulics (Bingham Plastic model) and torque and drag (Soft-String model) analyses. A key parameter in these evaluations is the mud motor differential pressure, which is used to accurately estimate the torque generated by the drill string and the additional pressure. Because it cannot be measured directly, it is derived from standpipe pressure measurements during

different operations. To calculate the mud motor differential pressures throughout, the rotating off-bottom and rotating on-bottom standpipe pressures are utilised and used for the dynamic simulations.

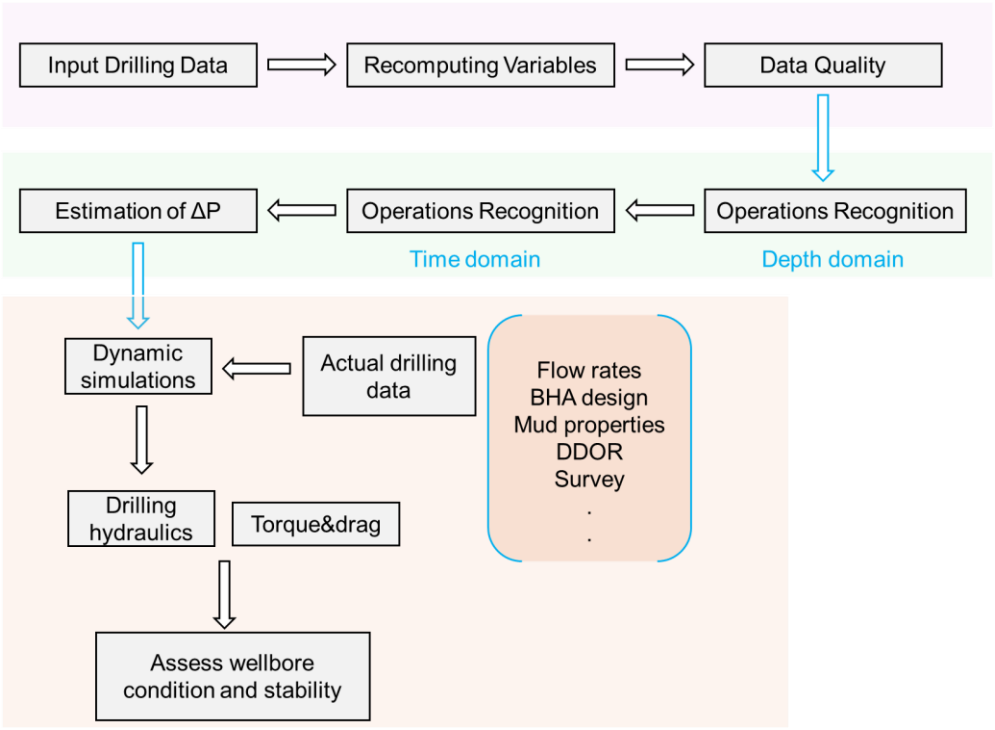
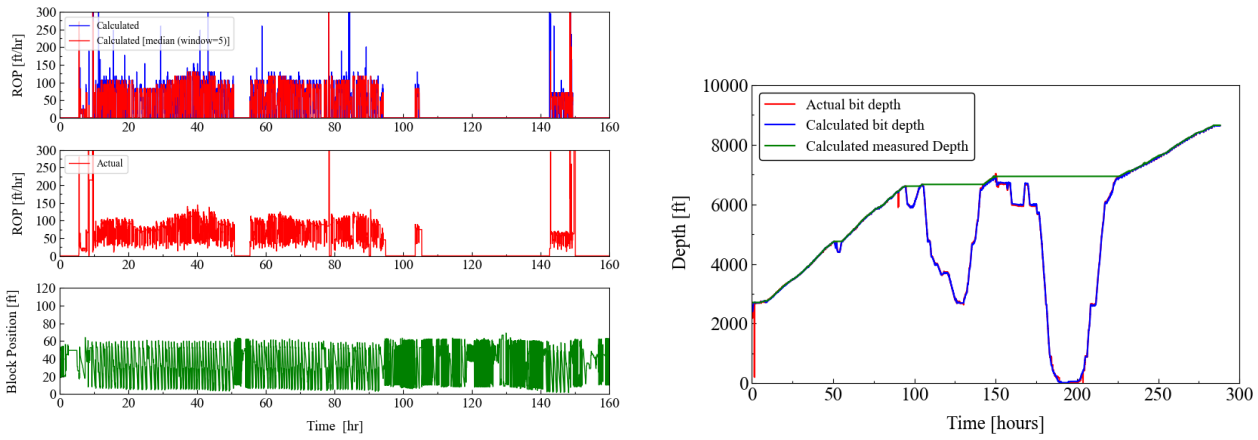


Figure 2. Overall workflow from data structure to modelling

4 RESULTS

4.1 Recomputing variables

As an example, the rate of penetration (ROP) and bit depth are calculated using the block position, with additional constraints including hook load and standpipe pressure. Figure 3a illustrates the computed rate of penetration (top), compared with the 'original' data supplied (middle), and the input block position (bottom). Figure 3b shows the calculated bit depth relative to the values in the dataset. The actual rate of penetration is seen to be averaged (including connection time) rather than the instantaneous values. Similarly, the drill bit and measured depth are computed at higher resolution, showing minor deviations from the original data (Figure 3b) that can influence the calculated drilling data.



(a) (b)

Figure 3. (a) Actual and calculated rate of penetration; (b) actual and calculated bit depth for the first part of the section of interest

4.2 Operations recognition

Drilling parameters are utilized to identify the operational mode for the current time step, including rotating/sliding drilling, rotating off-bottom, pumping off-bottom, slip to slip connection, etc. The current methodology focuses specifically on accurate captions of the drilling modes and rotating off-bottom. By utilising an automated operations recognition algorithm (Thonhauser, 2004; Thonhauser et al., 2007; El Afifi et al., 2015; Koulidis, 2023), each data point is assigned to a specific operation mode. The current algorithm utilizes data with a sampling frequency of 10 Hz.

4.3 Section 2715 – 6609 ft (deviation build)

The 12.25in section from 2715 - 6609 ft was drilled with two PDC drill bits (and two BHAs) and an oil-based mud (OBM) with an average density of 9.8 ppg, plastic viscosity of 34 cP and yield point of 24 lbs/100ft^2. The bottom hole assembly (BHA) consisted of a positive displacement motor (8 ¼" 7/8L-4.0stg) and the inclination started from 0 degrees and achieved 47 degrees. The used motor had a torque factor (c1) equal to 16 ft-lb/psi. The coefficients c2 and c3 (rotational factor) are defined to be -0.000013 and 0.155 RPM/gal, respectively. As illustrated in Figure 4, the section was drilled with a controlled rate of penetration (ROP) of approximately 100 ft/hr. In addition, after approximately 10 hr, the flow rate was increased and maintained at similar levels throughout the section.

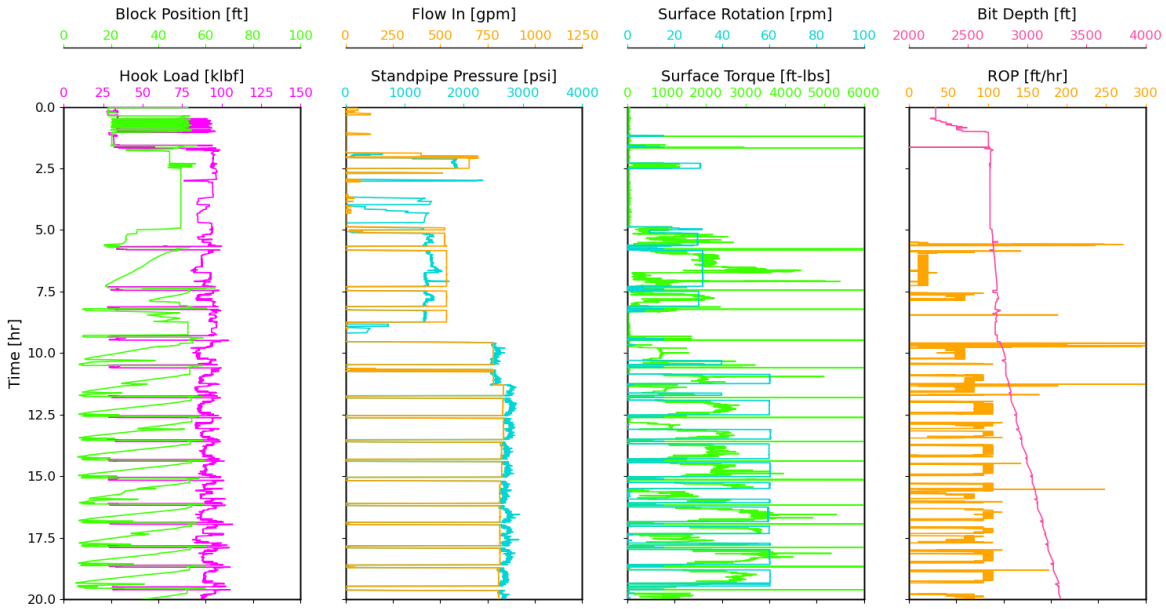
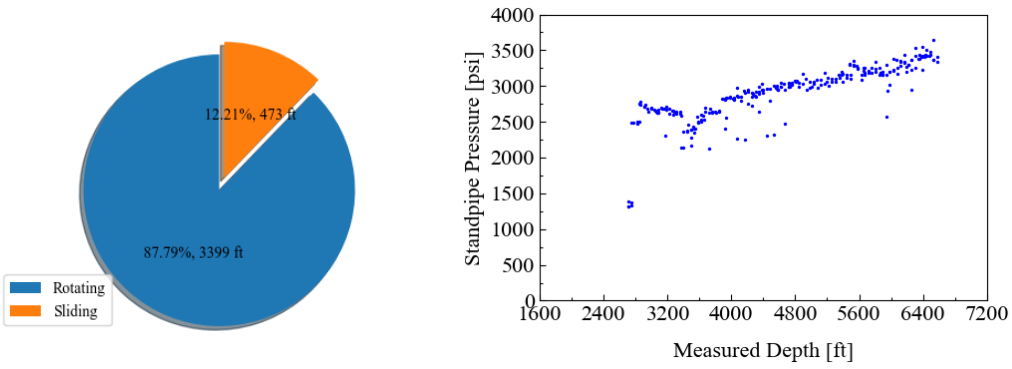


Figure 4. Visualization of the dataset showing a controlled ROP of approximately 100 ft/hr

As an input to the calculated torque, the drilling mode (rotating, sliding, rotating off-bottom) needs to be identified. It is seen that the majority of the interval was drilled with a rotating drilling (87.79%, 3399 ft), while 12.21% (473 ft) were sliding drilling intervals (Figure 5a) and several hundred rotating off-bottom operations were identified with the corresponding standpipe pressures presented in Figure 5b.



(a) (b)

Figure 5. (a) Rotating and sliding drilled depths; (b) Standpipe pressure during rotating off-bottom

The computed mud motor differential pressure and torque are shown in Figure 5 as a function of measured depth.

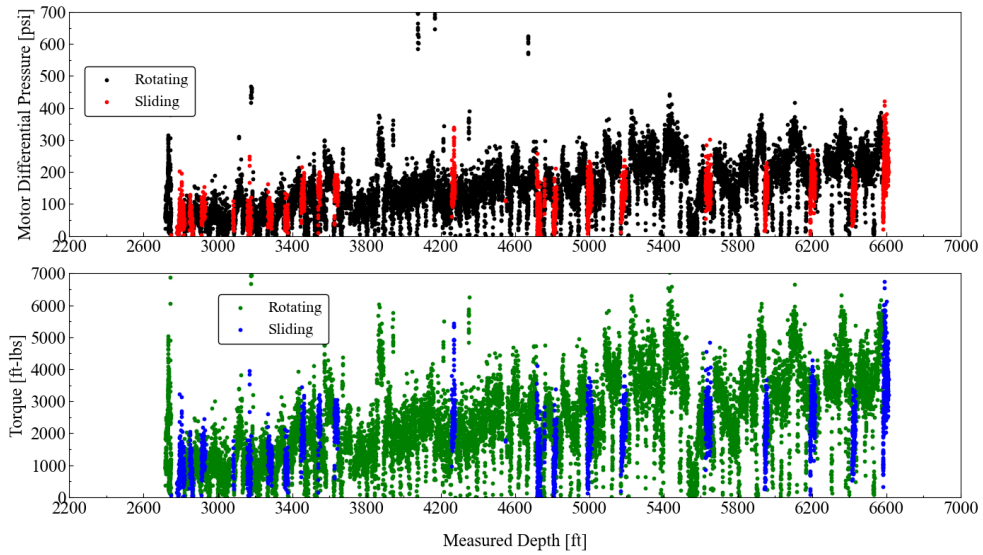
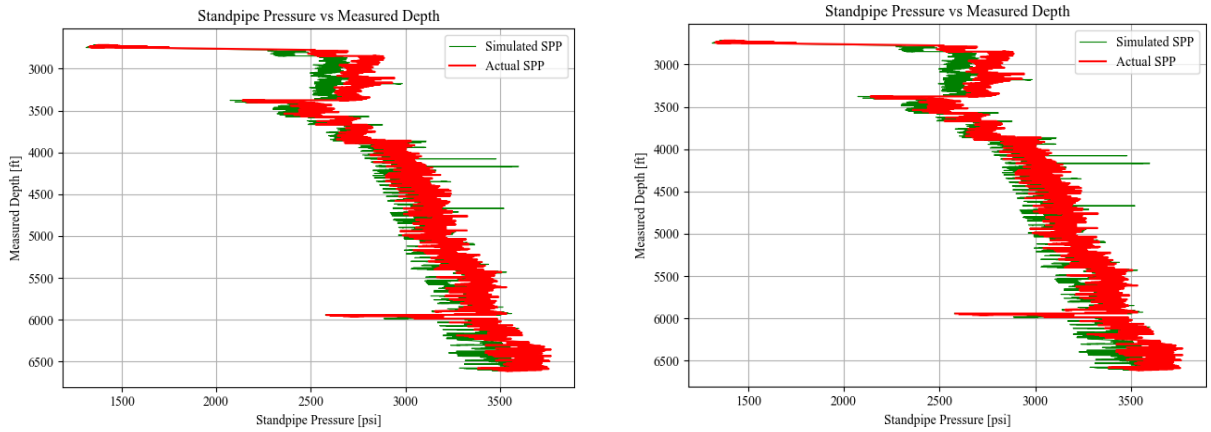


Figure 5. Estimated mud motor differential pressure and produced mud-motor torque

Figure 6 shows the standpipe pressure for the entire section, including the measured 'actual' flow rate (Figure 7a) and the additional variables, including fluid gain/losses, cuttings and mud motor differential pressure (Figure 7b). The results show good agreement with the actual standpipe pressure when including all variables, with some differences in the earliest interval from 2800 to 3300 ft. The slight increase in the actual SPP may be due to tight spots in the wellbore. Towards the end of the section, the actual standpipe pressure shows a slight increase relative to the simulated. Cavings were reported to be approximately 5861 ft to 6258 ft, and it was also challenging to perform sliding drilling between 6580 ft and 6610 ft. It is possible that the cavings contributed to these sliding difficulties, as their accumulation can restrict tool movement. This is also observed in Figure 6, where the motor torque during sliding drilling is significantly higher than before.



(a) (b)

Figure 6. Modelled standpipe pressure vs actual, using drilling data and BHA design. (a) Considers the actual flow rates and (b) considers the actual flow rates, gain/losses and mud motor differential pressure

The ECD was calculated for two scenarios. In Figure 8a, the calculation is based on the actual flow rate, and in Figure 8b, we adopted a similar approach to Figure 8a, accounting for the effect of cuttings. The results show that the reported ECD that was provided by the company is significantly higher than the modelled, probably due to cutting settlement, which was not included in these simulations.

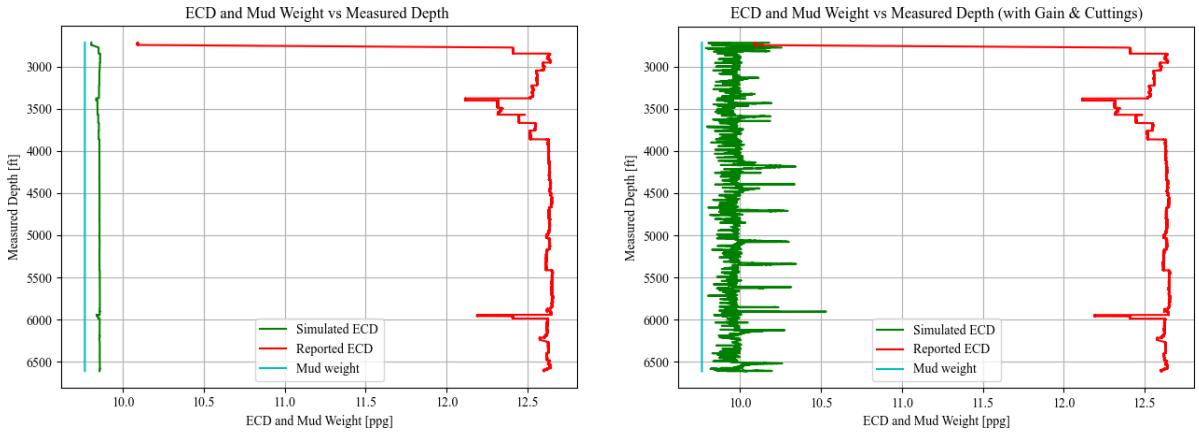


Figure 7. Modelled ECD vs actual for (a) considering the pressure losses for a clean wellbore (b) by implementing the effect of cuttings

Figure 8 shows the comparison between simulated and measured (actual) torque. In practice, additional torque is produced by poor hole cleaning, tight spots, and drill bit wear. By combining drilling data and dynamic modelling, differences can be examined as an indication of drilling issues, e.g. instabilities or features which can lead to instabilities. The modelled torque, considering the torque produced from the drill string and the mud motor, is slightly underestimated compared to the measured torque between 4000 and 5250 ft. The difference can be attributed to additional drag in the wellbore, induced by tight spots, which increase surface torque but do not significantly affect the standpipe pressure. Between 6400 ft and 6500 ft, both the measured SPP and the surface torque increase, indicating that cavings are affecting both variables. Toward the end of the section (after 5250 ft), the simulated and measured torque are similar, suggesting that the additional drag observed earlier was no longer present.

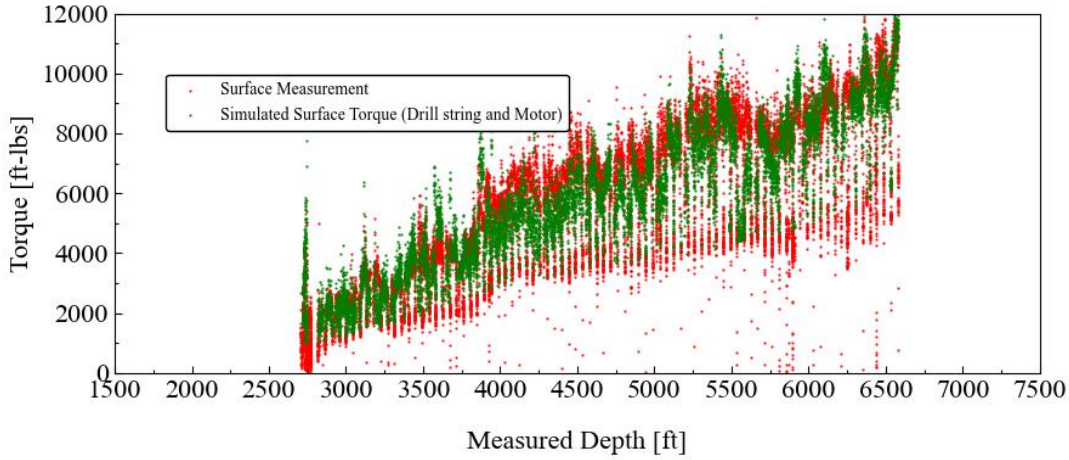


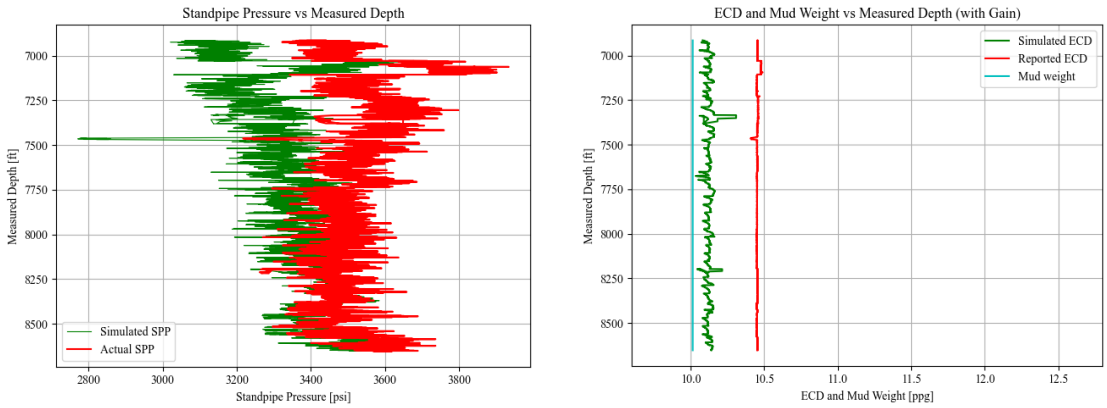
Figure 8. Modelled and measured surface torque at different drill bit depths. The friction factor for the entire open hole section was 0.27 and 0.15 for the cased hole. The sudden decrease in simulated torque at 5000 ft and 5500 ft indicates that the mud motor torque was not accurately captured

4.4 Section 6900 to 8652 ft

The same procedure and modelling are followed for the deeper section from 6900 to 8652 ft. An oil-based mud with an average density of 10 ppg, plastic viscosity of 28 cP and yield point of 23 lbs/100ft^2 was used.**Fehler! Verweisquelle konnte nicht gefunden werden.**

It is observed that simulated and actual standpipe pressure values differ (Figure 10a). In theory, as depth increases, pressure increases linearly for the same flow rate. The flow rate for drilling this section decreased from an average of 825 GPM in the previous interval to 783 GPM, with the surface pipe and equipment pressure losses assumed to remain the same. The actual standpipe pressure is approximately 300 psi higher than the simulated value at 6900 ft. Furthermore, the simulated SPP exhibits a clear increasing trend with depth, whereas

the actual SPP remains essentially constant throughout the interval after 7500 ft. This is further explored in Section 4.5.



(a) (b)

Figure 10. Modelled and actual standpipe pressure and ECD. The rapid increase of ECD is due to a high gain of approximately 400 L, which increases the annular flow rate

Due to the greater variability in the standpipe pressure and the resulting ECD, cuttings were not included in this analysis. Compared to the previous section, the ECD values are significantly closer (Figure 10b). At approximately 7300 ft, a rapid increase in the simulated ECD is observed, which is due to a wellbore fluid gain in the wellbore.

In comparison with the shallower section, the dynamic simulation demonstrated good agreement with the measured torque across the entire interval (Figure 11). In contrast to standpipe pressure, the torque values match well even in the initial section (7000 ft), where a 300 psi difference was observed in the SPP. Focusing solely on torque, the values follow a similar trend, but there are some noticeable differences, such as at 7300 ft, 7900 ft and 8460 ft, where significant torque spikes are observed. Specifically, at approximately 8460 ft, the torque exhibits a spike that persists for a certain depth, indicating for the first time a longer-range propagation of the disturbance within the wellbore.

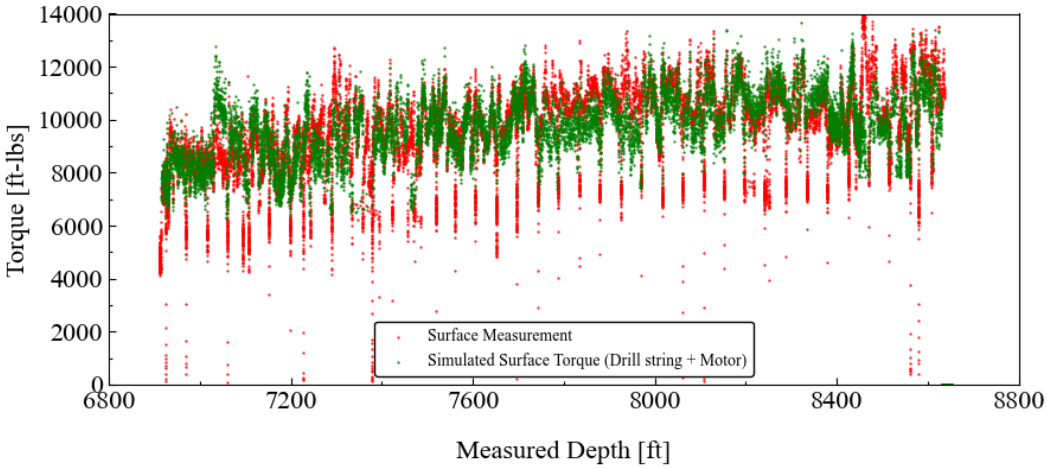


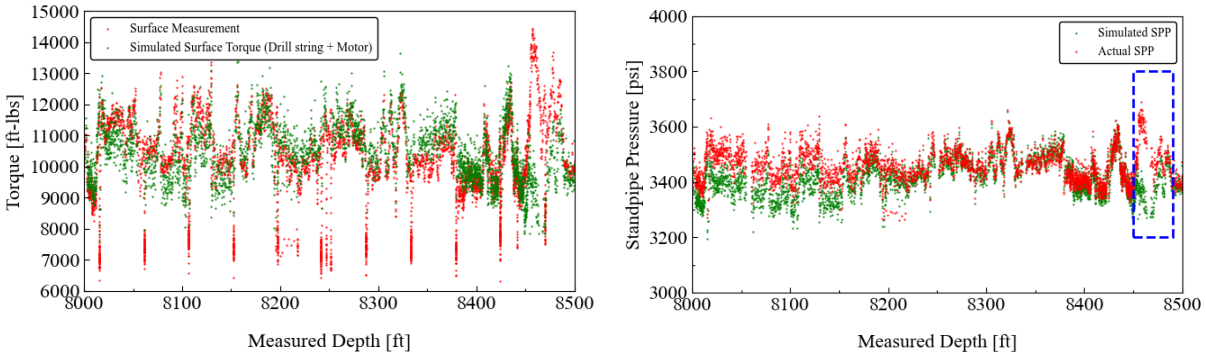
Figure 9. Modelled and actual torque. The friction factor for the entire open hole section was 0.27 and 0.15 for the cased hole

A closer examination of the estimated mud motor differential pressure, compared with the field measurements, reveals that in the initial part of the drilled section (at 7050 ft), the estimated values are higher than the actual measurements, whereas elsewhere they have more variability due to the higher resolution of measurements included in the simulation, but follow the trend well. For the interval from 7000 to 7050 ft, the flow rate during rotating off bottom with rotating drilling differed by 40 GPM, which was the cause of the difference. At approximately 7700 ft, a deviation between the simulated and actual torque is shown. The actual surface torque trend in Figure 11 appears to be reliable, with the simulated having underestimated the mud motor torque.

4.5 Integration of analytical results and field observations (DDOR)

Differences between torque and standpipe pressure can provide valuable insight into downhole conditions. Since the mud motor differential pressure is relatively consistent with the field measurements, it is not thought to be likely to be the primary factor influencing the observed differences between the SPP measurements and the simulation. As illustrated in Figure 10, the difference between the simulated and actual SPP shows a structural deviation rather than random variability. In addition, the modelled and measured torque values have a similar consistent trend, indicating good agreement between the simulation results and the field data, and the analysis utilized the actual flow rates and gains/losses. Therefore, the main factors that may explain the decrease in actual standpipe pressure with increasing depth are (1) drill bit nozzle erosion (2) hole enlargement and (3) temperature effects on the drilling fluid.

As mentioned, in an ideal situation, SPP increases with depth because the pressure losses both inside and outside the drill string increase linearly if the flow rate is constant. **Fehler! Verweisquelle konnte nicht gefunden werden.** show that the flow rate was constant throughout the entire drilled interval. The model torque captures the trends from 8400 ft to 8450 ft, including the spikes that originate from the mud motor (Figure 12). There were also two additional torque spikes at 7300 ft and 7900 ft. Nevertheless, occasional spikes in torque and SPP are not unusual, especially if the values subsequently return to their expected ranges. But the torque and SPP spikes at 8460 ft indicate a more significant effect from cavings in the wellbore, as highlighted in Figure 12. Throughout the interval, the DDOR reported that small claystone cuttings were observed in the shakers.



(a) (b)

Figure 12. Comparison of actual and simulated torque and standpipe pressure over the zoomed depth interval between 8000 to 8500 ft

In case of severe tight spots, washouts, or pack-offs, the torque and standpipe pressure tend to increase progressively and remain elevated over time, due to increasing mechanical drag and restriction in the wellbore. For the deeper part of the section, after each stand was drilled, a full single backreaming was performed to improve the hole condition. It is a short-term, not a permanent, solution for wellbore stability or quality. Conversely, occasional spikes in torque or SPP that subsequently return to expected values are characteristic of transient operational effects rather than an actual onset of wellbore instability or collapse. Nevertheless, as was stated, the torque and SPP spikes at 8460 ft are more persistent.

DEL-GT-02 eventually suffered wellbore collapse, requiring two sidetracks. A study performed by Mehranpour et al. (2024) indicated that the failure was likely related to bedding-layer orientation and mud infiltration rather than general wellbore instability. From a modelling perspective, some signs were detected, including torque difference between 4000 ft to 5250 ft, SPP trend throughout the section (below 6900 ft) and torque and SPP spikes near the end of the section. However, the cavings reported throughout the section, combined with the indications from the modelling, suggest some wellbore instability. This highlights the importance of integrating all variables when evaluating wellbore stability.

5 CONCLUSIONS

The findings demonstrate that automated data-driven analysis, when combined with physics-based modelling, provides an effective tool for diagnosing wellbore conditions. The main highlights of this study can be summarized as follows:

- Considering both the differential pressure and the torque generated by the mud motor provides a more accurate comparison with the actual measurements of torque and standpipe pressure.

- Incorporating a dynamic drilling model significantly enhances drilling analysis by capturing dynamic fluctuations and real-time interactions between drilling parameters, enabling a comprehensive understanding of wellbore conditions and operational responses.

- For the upper section, the actual values of both torque and standpipe pressure are in good agreement with the simulated values. Early torque differences were due to drag from tight spots, while concurrent SPP and torque increases at 6,400–6,500 ft indicate cavings.

- The comparison between measured and simulated parameters indicates some signs of wellbore instability but no large evidence of progressive torque or standpipe pressure buildup, which would typically signify severe tight spots, washouts, or pack-offs. This is partly because backreaming prevented these issues from developing.

- The measured standpipe pressure shows a flatter trend with depth compared to the simulated response, suggesting lower frictional losses potentially due to some partial hole enlargement or model underestimation of the frictional pressure losses.

- The close correlation between actual and simulated torque indicates that, overall, the wellbore condition remains consistent with the modelled expectations, although some events suggest minor instability in specific intervals.

- The integration of minor modelling indications with the reported cavings indicates the presence of some wellbore instability.

The proposed methodology can be applied to other geothermal wells by utilizing well-specific drilling data and operational conditions. The geothermal energy sector requires robust and automated frameworks to enable early detection of drilling issues, support informed operational decision-making, and reduce non-productive time.

Acknowledgements
The partners of the GTD project are gratefully acknowledged, as is the EPOS-NL project funded from the Dutch Research Council (NWO) via the Dutch national research infrastructure for solid Earth sciences (project number 184.034.005).

REFERENCES

Cayeux, E. and Daireaux, B. : Early detection of drilling conditions deterioration using real-time calibration of computer models: field example from North Sea drilling operations, SPE/IADC Drilling Conference and Exhibition, Amsterdam, the Netherlands (2009).

Chi, Y., V. Kemajou, Rajan , A. and Samuel, R. : Cloud-Based Real-Time Well Engineering: Coupling Torque-And-Drag and Uncertainty Modeling, SPE/IADC International Drilling Conference and Exhibition, Stavanger, Norway (2023).

El Afifi, S., Albassam , B. and Fahmy, F. A. : Enhance the Drilling & Tripping Performance on Automated Rigs with fully automated performance measurement, SPE Middle East Intelligent Oil and Gas Symposium, Abu Dhabi, UAE (2015).

Koulidis, A.: Drilling Mechanics: In-Cutter Sensing and Physics-Based Modelling for Drilling Optimization, King Abdullah University of Science and Technology, Saudi Arabia (2023).

Koulidis, A., Abdullatif , M. and Ahmed, S. : Drilling monitoring system: mud motor condition and performance evaluation, SPE Middle East Oil and Gas Show and Conference, Manama, Bahrain (2023).

Koulidis, A. and Ahmed, S. : Positive Displacement Motor Condition and Performance Prediction Using Surface and Downhole Sensor Data, Exploring the World of Drilling, (2024).

Marbun, B. T. H., Widiyanto , Y. A. and Kurnianto, B. E. : Feasibility study of casing while drilling application on geothermal drilling operation, Thirty-Ninth Workshop on Geothermal Reservoir Engineering, Stanford, California, USA (2014).

Mehranpour, M.H, Wiprut, D., Godfrey, S., Vardon, J.P, Laumann, S., Barnhoorn, A., Ursem, L. J. and Schravendijk, B.: Post Drill 1D Geomechanical Study of the TU Delft Geothermal Doublet, International Geomechanics Conference, Kuala Lumpur, Malaysia (2024).

McKinsey&Company: McKinsey & Company, (2025) https://www.mckinsey.com/industries/energy-and-materials/our-insights/global-energy-perspective

Montes, A. C., Ashok, P. , van Oort, E. , Leš, B. , Mullendore , M. and Limaye, S. : Casing Run Failure Avoidance Through Automated Assessment of Borehole Quality, *SPE Journal,* (2025), 1–24.

Ng, M. T., Lum, T. , Yeap, F. , Abdul Talib, S. a. H. , Zainal Abiddin , M. S. and Hooi, E. W. : Real Time Operation Centre Monitoring and Optimizations in Highly Deviated Deepwater Development Wells in Malaysia, Abu Dhabi International Petroleum Exhibition & Conference, Abu Dhabi, UAE (2019).

Richard, B., Saarani, M. S. , Sulaiman, S. , Meor Hashim, M. M. H. , Arriffin , M. F. and Ghazali, R. : Delivering Proactive Real Time Drilling Decision for Extended Reach Drilling Well via Dynamic Trend-Based Monitoring System, SPE Asia Pacific Oil & Gas Conference and Exhibition, Adelaide, Australia (2022).

Samuel, R., Kumar , K. and Nakhle, A. : Casing (Tubular) Runnability Indicator While Drilling With Real Time Drilling Data, SPE/IADC Asia Pacific Drilling Technology Conference and Exhibition, Bangkok, Thailand (2024).

Thonhauser, G.: Using real-time data for automated drilling performance analysis, *Oil Gas European Magazine,* **30,** (2004).

Thonhauser, G., Wallnoefer, G. , Mathis , W. and Ettl, J. : Use of real-time rig-sensor data to improve daily drilling reporting, benchmarking, and planning—a case study, *SPE Drilling & Completion,* **22,** (2007), 217–226.

Van Oort, E.: On the physical and chemical stability of shales, *Journal of Petroleum Science and Engineering,* **38,** (2003), 213–235.

Vardon, P. J., Abels, H. A. , Barnhoorn, A. , Daniilidis, A. , Bruhn, D. , Drijkoningen, G. , Elliott, K. , van Esser, B. , Laumann , S. and van Paassen, P. : A research and energy production geothermal project on the TU Delft campus: Project implementation and initial data collection, 49th Workshop on Geothermal Reservoir Engineering, Stanford, California, USA (2024).

Vardon, P. J., Laumann, S. J. , van Esser, B. T. M. , Ursem, L. J. H. , van Schravendijk, B. , Meleza, L. V. , Barnhoorn, A. , Abels, H. A. , Vondrak , A. G. and Drijkoningen, G. G. : End-of-Well Science Programme Report DEL-GT-01 and DEL-GT-02: TU Delft campus geothermal project (2024).

Voskov, D. V., Abels, H. A. , Vardon, P. J. , Vargas Meleza, L. , Verschuur, D. J. , Vondrak, A. G. , Barnhoorn, A. , Chen, Y. , Daniilidis , A. and Bruhn, D. F. : A research and production geothermal project on the TU Delft campus, 49th Workshop on Geothermal Reservoir Engineering, Stanford, California, USA (2024).

Wang, L., Shen , Q. and Wang, G. : Prediction of Cuttings-Induced Annular-Pressure Loss in Extended-Reach Wells, *Fluid Dynamics & Materials Processing,* **19,** (2023).

Yarim, G., Ritchie , G. M. M. and May, R. B. B. : A Guide to Successful Backreaming: Real-Time Case Histories, *SPE Drilling & Completion,* **25,** (2010), 27–38.

Zoback, M. D.: Reservoir geomechanics, (2010).